scientific reports

Check for updates

OPEN

Development of eco-friendly activated carbon from olive pits for the adsorption of tartrazine with isotherm kinetic and thermodynamic studies

Abderrahmane Remil[1], Abdelkrim Bendoukha Reguig[1], Mokhtar Saidi[1], Abdelghani Bouchama[2,3], Mohammed El Amine Monir[4], M. Fatmi[5]✉, S. Alomairy[6], Talal M. Althagafi[6], Aseel Smerat[7], Mustafa Jaipallah Abdelmageed Abualreishh[8] & Murat Yaylacı[9,10]

Synthetic dyes discharged into water bodies pose a persistent environmental threat owing to their resistance to natural degradation, toxicity, and long-term ecological impact. In this study, discarded olive pits were valorized as a lignocellulosic precursor for the production of activated carbon through phosphoric acid activation. Multiple analytical tools including pHpzc, FTIR, SEM, XPS, and XRD—were used to examine the structural, physicochemical, and morphological characteristics of the prepared material. The influence of key process variables on Tartrazine uptake was assessed through a series of batch-mode experiments, including pH, initial dye concentration, adsorbent dose, contact time, and temperature. Maximum adsorption was achieved in acidic medium (pH = 2) using an adsorbent dose of 40 mg, an initial Tartrazine concentration of 40 mg L^{-1}, a contact time of 24 h, and a temperature of 298 K. The maximum adsorption capacity reached 47.18 mg g^{-1} according to the BET model, while the pseudo-second-order kinetic model provided the best fit (R^2 = 0.9996) with an experimental Qe value of 31.39 mg g^{-1}. Thermodynamic parameters ($\Delta H°$ = − 10328 J mol^{-1}; $\Delta G°$ = − 1409 to − 1794 J mol^{-1}) confirmed that the process is exothermic and spontaneous. The results of the pseudo-second-order kinetic model and Thermodynamic analysis showed that the process is a mixed adsorption mechanism dominated by physisorption. These findings collectively establish H3PO4-activated olive pit carbon as a high-performance, cost-effective, and environmentally viable material for Tartrazine decontamination from water matrices.

Keywords Olive kernels, Raw carbon, Tartrazine, Adsorption, Phosphoric acid activation, Water treatment

The widespread discharge of synthetic colorants into aquatic systems raises serious public health concerns, given their inherent toxicity, limited natural degradation, and cumulative effects on water quality. Among these dyes, Tartrazine (E102), an anionic azo dye widely utilized in food, pharmaceutical, and textile industries, has attracted significant attention. This growing concerns stems from its documented potential to cause harmful effects on aquatic ecosystems, environmental quality, and possible risks to human health[1]. Documented health effects linked to Tartrazine intake encompass allergic manifestations, respiratory issues, migraine episodes,

[1]Laboratory of Organic, Macromolecular Chemistry and Materials, University of Mustapha Stambouli, Mascara, Algeria. [2]Center for Scientific and Technical Research in Physical-Chemical Analyses (CRAPC), BP 384, Bousmail, Algeria. [3]Technical Platform for Physical-Chemical Analyses (PTAPC), Mostaganem, Mostaganem 27000, Algeria. [4]Faculty of the Exact Sciences, Mustapha Stambouli, University of Mascara, B.P. 305, Mascara 29000, Algeria. [5]Research Unit on Emerging Materials (RUEM), University Ferhat Abbas of Setif 1, Setif 19000, Algeria. [6]Department of Physics, College of Sciences, Taif University, P.O. Box 11099, Taif 21944, Saudi Arabia. [7]Hourani Center for Applied Scientific Research, Al-Ahliyya Amman University, Amman 19328, Jordan. [8]Department of Chemistry, College of Sciences, Northern Border University, P.O. Box 1321, Arar 91431, Saudi Arabia. [9]Department of Civil Engineering, Recep Tayyip Erdogan University, 53100 Rize, Türkiye. [10]Turgut Kıran Maritime Faculty, Recep Tayyip Erdogan University, 53900 Rize, Türkiye. ✉email: fatmimessaoud@yahoo.fr

behavioral disturbances in children, and possible neurotoxic consequences. Environmentally, its high low biodegradation and chemical stability lead to persistence in aquatic systems, where it can significantly inhibit natural photosynthesis, reduce dissolved oxygen levels, and exert toxic effects on various aquatic organisms, thereby disturbing ecological balance. Conventional remediation strategies coagulation-flocculation, chemical oxidation, biological degradation have been widely applied, yet their practical utility is often hampered by elevated operational costs and technical constraints. Adsorption has therefore emerged as an efficient and economical alternative for removing organic pollutants from wastewater[2]. Among adsorbents, activated carbon stands out for its remarkably high specific surface area, highly developed pore network, and diverse surface functionalization. Recently, increasing interest has focused on biomass-derived adsorbents because of their low cost, renewability, and environmental sustainability. Agricultural wastes have been extensively investigated for pollutant removal, showing promising adsorption performance while contributing to waste valorization and environmental protection[3]. Numerous studies have confirmed that agricultural waste–based adsorbents (e.g., Luffa acutangula peels, Punica granatum seeds, Neolamarckia cadamba leaves, rubber seed pericarp) are efficient, reusable, and cost-effective for removing various dyes (methylene blue, crystal violet, methylene green) and organic pollutants such as diclofenac sodium, with adsorption behavior often following Langmuir isotherm models and pseudo-second-order kinetics[4–7]. Advanced oxidation processes (e.g., persulfate activation with nZVI) and modified carbon-based composites (AC-nZVI, magnetic Fe_3O_4/zeolite) have also demonstrated high efficiency for dye removal (Acid Blue 113, methylene blue), humic acid, and pharmaceutical compounds such as metronidazole, with removal efficiencies reaching 95–100% and adsorption following pseudo-first-order or pseudo-second-order kinetics[8–14]. These findings collectively confirm that carbon-based and modified adsorbents represent highly effective and sustainable materials for water and wastewater treatment applications. Other biomass-derived adsorbents such as spent coffee grounds (crystal violet, Cr(VI)), sugarcane bagasse (malachite green, up to 97% removal), and argan nut shells (malachite green oxalate) have also shown excellent adsorption performance with Langmuir/Freundlich isotherm behavior, pseudo-second-order kinetics, and spontaneous, often exothermic, thermodynamic profiles, confirming the potential of agricultural wastes for sustainable wastewater treatment[15–18]. Carpobrotus edulis has also been successfully used as a low-cost biosorbent for phosphate ions (up to 888.9 mg/g after acid modification), methylene blue (153.9 mg/g after alkali treatment), and crystal violet (166.6 mg/g), with adsorption following Langmuir isotherm behavior and pseudo-second-order kinetics, and good regeneration ability[19–21]. In contrast to previous studies, the present work focuses on the valorization of olive pits collected from western Algeria as a sustainable precursor and low-cost for activated carbon preparation using H_3PO_4 chemical activation. The originality of this study lies in combining detailed surface characterization (pHpzc, FTIR, SEM, XRD, and XPS) with comprehensive adsorption investigations of Tartrazine, an anionic azo dye that has received limited attention compared to other dyes. Furthermore, the simultaneous evaluation of isotherm, kinetic, and thermodynamic behaviors provide more comprehensive insight into the underlying adsorption mechanism, highlighting the strong potential of the prepared activated carbon for practical wastewater treatment applications. Olive pits, an abundant by-product of the olive oil industry, constitute a low-cost and renewable lignocellulosic precursor material for the sustainable production of activated carbon, In particular. Chemical activation using phosphoric acid (H_3PO_4) effectively enhances surface functionality and pore development by generating micro- and mesoporous structures and introducing oxygenated and phosphate groups[22]. Several studies have demonstrated the high efficiency of olive pit–derived Activated Carbon for removing inorganic and organic contaminants, highlighting the sustainability of this approach[23]. The scientific novelty and originality of this work lies in the valorization of locally available olive pits from western Algeria as a sustainable material for production of activated carbon combined with comprehensive surface characterization (FTIR, SEM, XRD, XPS, and pHpzc) and a complete adsorption investigation of Tartrazine, a relatively less-studied anionic azo dye. Unlike previous studies, this work integrates BET multilayer isotherm modeling with kinetic, thermodynamic, and mechanistic analyses in a single framework, providing deeper insight into the adsorption process and demonstrating the strong potential of olive pit–derived activated carbon for large scale and real-world application wastewater treatment applications.

Materials and methods

Materials

Tartrazine (E-102, 89% purity) served as the model pollutant. Chemical activation was performed using orthophosphoric acid (H3PO4, 40%), while pH regulation was carried out with NaOH (≥ 98%) and HCl (37%) solutions, and sodium chloride (NaCl, ≥ 99%) for pHpzc determination. The main physicochemical properties of Tartrazine are summarized in Table 1. All chemicals employed in this study were of analytical grade purity and were used directly as received from the supplier without any additional purification steps. Distilled water was systematically used in all experimental procedures to ensure consistency. Olive pits, obtained from the food industry were used as precursors for Activated Carbon preparation.

Preparation of Activated Carbon

Following collection, the raw pits underwent sequential hot-water and distilled-water washing to eliminate surface impurities, after which the samples were subsequently oven-dried at 110 °C over a 24-hour period. A preliminary grinding and coarse sieving step were performed to eliminate unwanted particles. Thermal carbonization was performed in a muffle furnace using a covered ceramic crucible with restricted headspace, thereby establishing an auto-generated reducing atmosphere that suppressed oxidation. A controlled heating ramp of 10 °C/min brought the system to a final pyrolysis temperature of 700 °C, which was sustained for 120 min. Surface area development and pore formation were promoted by impregnating 10 g of carbonized material with solution (100 mL of 40% H_3PO_4) under continuous mechanical agitation for 24 h. Excess acid was neutralized by washing the impregnated solid with 0.1 M NaOH, followed by repeated distilled water rinsing

Property	Value
Chemical name	Tartrazine
Molecular formula	$C_{16}H_9N_4Na_3O_9S_2$
Molecular weight	534.36 g/mol
Dye type	Anionic azo dye
CAS number	1934-21-0
Λmax	427 nm
Solubility	Highly soluble in water
Appearance	Orange powder
Application	Food, pharmaceutical, textile
Charge	Negative

Table 1. Main physicochemical characteristics of Tartrazine.

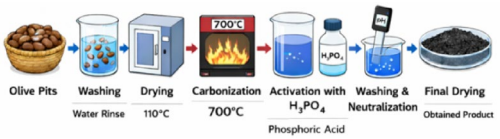


Fig. 1. Schematic representation of the synthesis process of activated carbon from olive pits.

until the effluent reached a near-neutral pH (~7). Finally, the Activated Carbon was dried at 110 °C for 24 h and stored in a desiccator for later use[24]. The overall synthesis procedure of activated carbon from olive pits is schematically illustrated in Fig. 1.

Characterization methods

The physicochemical and structural properties of the prepared Activated Carbon were characterized using several complementary analytical techniques. Fourier Transform Infrared Spectroscopy (FTIR) was conducted using a Perkin-Elmer spectrophotometer within the 400–4000 cm^{-1} range to identify surface functional groups[25]. Scanning Electron Microscopy (SEM) measurements were conducted on an FEI Nova Nano SEM 230 microscope operating at 8 kV to observe morphology, pore size and distribution, and surface roughness[26]. X-ray Diffraction (XRD) was used to evaluate the crystalline or amorphous structure, employing a Bruker D4 ENDEAVOR diffractometer equipped with a CuKα radiation source (λ = 1.5406 Å) and a graphite monochromator[27]. (XPS) ont fourni des informations complètes et approfondies qui ont permis une compréhension précise de la composition de surface et des caractéristiques chimiques du matériau using a Thermo Scientific K-Alpha spectrometer (Al Kα, 1486.6 eV) equipped with a hemispherical analyzer[28]. Additionally, the point of zero charge (pHpzc) was determined by the pH equilibrium method. A series of solutions (50 mL) were prepared with initial pH values ranging from 2 to 12 adjusting with HCl or NaOH solutions. Each solution was mixed with 0.05 g of Activated Carbon and stirred for 24 h at 25 °C. The pHpzc was defined as the initial pH for which ΔpH (pHf – pHi) equals zero. The ΔpH values were graphed versus the initial pH to identify the (pHpzc)[29].

Adsorption experiments

To evaluate the uptake efficiency and adsorption performance of the Activated Carbon derived from olive pits, Tartrazine (E-102) was chosen as a model contaminant adsorbate due to its widespread use in food, pharmaceutical, and textile industries. This synthetic anionic dye appears as an orange powder with a purity of 89%. A stock solution of 1000 ppm was obtained by dissolving 1 g of Tartrazine in 1 L of distilled water and stirred for 24 h to ensure homogeneity. From this solution, serial dilutions were made to obtain different concentrations from 1 to 40 mg/L. The maximum absorption wavelength (λmax) was determined using UV-visible spectrophotometry within the 400–500 nm range and found to be 427 nm[30]. The absorbance of each diluted solution was measured at this wavelength, allowing the establishment of a calibration curve (A = f(C)), later used to determine residual Tartrazine concentrations after adsorption. The adsorption experiments were conducted using both raw and activated olive-pit carbon. Solutions of 40 ppm were prepared from the 1000 ppm stock solution. In 50 mL test tubes, 2 mL of Tartrazine solution was diluted with distilled water and mixed with 40 mg of the adsorbent. All suspensions were agitated on a reciprocating shaker for 24 h a duration established in preliminary tests as sufficient to guarantee equilibrium attainment across all tested conditions, followed by centrifugation three times at 10,000 rpm for 15 min[31]. Residual dye concentrations were measured at λmax = 427 nm using a UV-Visible spectrophotometer. Each experiment was replicated three times under consistent operating conditions; Mean values are reported with an associated relative standard deviation not exceeding ± 5%.

Analytical procedures

The equilibrium concentration (Ce) was determined from the calibration curve, and the adsorbed quantity at equilibrium (Qe) was calculated using the equation:

$$\mathrm{Qe} = \frac{\mathrm{V}}{\mathrm{m}} . \ (\mathrm{C0} - \mathrm{Ce}) \tag{1}$$

where Ce (mg/L) and C0 (mg/L) represent the equilibrium and initial concentrations, respectively, m (g) the mass of carbon used, and V (L) the volume of solution.

To optimize the decolorization process, the influence of various parameters on Tartrazine adsorption was examined. The parameters studied included pH, adsorbent dosage, initial dye concentration, temperature, and contact time[32]. The adsorption equilibrium data were analyzed using Langmuir, Freundlich, and Brunauer–Emmett–Teller (BET) isotherm, Temkin models. Freundlich describes multilayer adsorption on heterogeneous surfaces with non-uniform energy distribution, whereas Langmuir assumes monolayer adsorption on homogeneous surfaces with identical active sites.

The Langmuir model is now presented with its linear equation:

$$\frac{\mathrm{Ce}}{\mathrm{Qe}} = \frac{1}{\mathrm{KL}.\mathrm{Q_m}} + \frac{\mathrm{Ce}}{\mathrm{Q_m}} \tag{2}$$

where Q_m (mg/g) is the maximum adsorption capacity and K_L (L/mg) is the Langmuir constant related to adsorption affinity.

The Freundlich model, which describes multilayer adsorption on heterogeneous surfaces, is presented with its linear form:

$$\ln\mathrm{Qe} = \frac{1}{\mathrm{n}}\ln\mathrm{Ce} + \ln\mathrm{KF} \tag{3}$$

where K_F is the Freundlich constant and 1/n indicates adsorption intensity.

The BET isotherm model was expressed by the following equation:

$$\frac{\mathrm{C_e}}{\mathrm{Q_e}\,(\mathrm{C_s} - \mathrm{C_e})} = \frac{\mathrm{C_{BET}} - 1}{(\mathrm{Q_m}\mathrm{C_{BET}})}.\frac{\mathrm{C_e}}{\mathrm{C_s}} + \frac{1}{\mathrm{Q_m}\mathrm{C_{BET}}} \tag{4}$$

where Ce (mg/L) is the equilibrium concentration, Cs is the saturation concentration, Qe (mg/g) is the amount adsorbed at equilibrium, Qm (mg/g) is the maximum adsorption capacity, and C_{BET} is the BET constant related to the adsorption energy.

Linear plots of Qe versus Ce were used to determine the characteristic constants of each model, providing insights into the adsorption mechanisms between Tartrazine and Activated Carbon under optimal and ambient conditions[33]. The adsorption kinetics were analysed using several classical models, including pseudo-first-order (Lagergren), pseudo-second-order, Elovich, and intraparticle diffusion models. These analyses helped describe the adsorption rate and elucidate the mechanisms controlling mass transfer within the system[34]. The pseudo-first-order kinetic model presumes that the adsorption rate is proportional to the number of unoccupied sites and is expressed as:

$$\mathrm{Ln}\,(Q_e - Q_t) = \mathrm{Ln}\,(Q_e) \tag{5}$$

where Qt (mg/g) and Qe (mg/g) are the adsorption capacities at time t and at equilibrium, respectively, and K_1 (h^{-1}) is the constant of pseudo-first-order rate.

The pseudo-second-order model presumes that chemisorption may be the rate-controlling step and is given by:

$$\frac{t}{Qt} = \frac{1}{K2Qe^2} + \frac{1}{Qe} \cdot t \tag{6}$$

where K_2 (g/mg h) is the pseudo-second-order rate constant.

The Elovich model describes adsorption on energetically heterogeneous surfaces and is expressed as:

$$\mathrm{Qt} = \frac{1}{\beta}\,\ln\mathrm{t} + \frac{1}{\beta}\,\ln\left(\alpha\,\beta\right) \tag{7}$$

where α (mg/g h) represents the initial adsorption rate and β (g/mg) is related to surface coverage and activation energy.

The intraparticle diffusion model is defined as:

$$Q_t = C + K_i dt^{1/2} \tag{8}$$

where K_id (mg/g $h^{1/2}$) is the constant of intraparticle diffusion rate and C reflects the boundary layer thickness.

Thermodynamic studies were performed at various temperatures (24, 30, 35, and 40 °C). The thermodynamic parameters ΔS (entropy), ΔH (enthalpy), and ΔG (Gibbs free energy) were calculated to determine the order/

disorder changes within the adsorption system, the energetic nature (exothermic or endothermic), and the spontaneity of the adsorption process[35].

The thermodynamic parameters were calculated using the following equations:

$$\Delta G^{\circ} = -RT \ln K_c \tag{9}$$

$$\ln \mathrm{Kc} = -\frac{\Delta \mathrm{H}^{\circ}}{\mathrm{R}} \cdot \frac{1}{\mathrm{T}} + \frac{\Delta \mathrm{S}^{\circ}}{\mathrm{R}} \tag{10}$$

where ΔS° (J/mol·K) is the entropy change, ΔH° (J/mol) is the enthalpy change, ΔG° (J/mol) is the Gibbs free energy change, Kc is the equilibrium constant, R is the universal gas constant (8.314 J/mol·K), and T is the absolute temperature (K).

Results and discussion

FTIR analysis

FTIR analysis of the raw olive pit material (NO) discloses spectral features typical of lignocellulosic structures, including a broad hydroxyl stretching band (3650–3750 cm^{-1}) associated with cellulose/hemicellulose and a carbonyl absorption near 1700 cm^{-1} attributable to carboxylic functionalities, a signal at 1540 cm^{-1} attributed to the aromatic rings of lignin, as well as a distinct peak at 670 cm^{-1} corresponding to the aromatic C–H bonds (Fig. 2). These signals reflect a high content of oxygenated groups. After carbonization, the intensity of these bands decreases sharply, indicating the thermal decomposition of volatile compounds. In contrast, the persistence of the band at 1600 cm^{-1} testifies to the stability of the carbonized aromatic structures. Upon H3PO4 activation, two new absorption bands emerge at 1292 and 1120 cm^{-1}, characteristic of P=O stretching and P–O–C linkages, which are diagnostic of phosphorus incorporation onto the carbon framework. The functional groups identified on the activated carbon surface play a crucial role in the adsorption of Tartrazine. Hydrogen bond formation between Tartrazine molecules and the surface hydroxyl, carbonyl, and carboxyl functionalities, combined with π-π conjugation between the graphitic carbon backbone and the dye's aromatic rings, collectively drive the adsorption process. In acidic conditions, the protonation of surface functional groups lead to the generates positively charged sites, which enhances electrostatic attraction toward the anionic Tartrazine molecules. In addition, phosphate-related groups introduced by H_2PO_4 activation increase surface polarity and provide additional active sites for adsorption. These synergistic interactions, namely electrostatic forces, hydrogen-bond formation, and π–π stacking between aromatic structures, play a major role in enhancing the adsorption efficiency of the activated carbon. These structural transformations give Activated Carbon developed porosity and active groups capable of interacting with organic molecules such as Tartrazine via hydrogen bonds, π–π and electrostatic interactions. Comparable results have been reported in earlier studies, where phosphoric acid activation was shown to promote the formation of phosphate and oxygen-containing functional groups, enhancing surface polarity and improving the adsorption performance toward organic pollutants through electrostatic attraction and π–π interactions[36,37].

SEM analysis

Pre-adsorption SEM imaging of the activated carbon reveals a markedly irregular surface topology featuring an interconnected network of pores with varied geometry (Fig. 3). The micrographs highlight the presence of interconnected macropores and mesopores, as well as cavities of various sizes, providing a large specific surface area conducive to adsorption. The rough and fissured texture suggests the existence of multiple active sites promoting interaction with tartrazine molecules. These morphological characteristics confirm the ability of the material to effectively trap organic dyes, particularly due to the availability of accessible pores and the irregular nature of its surface[38–40]. However, a closer examination of the SEM image indicates that the surface is predominantly irregular and fragmented, with rough edges, fissures, and void-like structures rather than clearly defined cylindrical pores. The observed morphology suggests that chemical activation mainly induced structural disruption and surface roughening, which contribute to the creation of adsorption sites and facilitate dye diffusion toward the internal structure of the carbon.

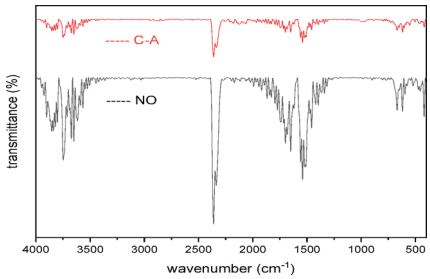


Fig. 2. FTIR spectrum of the raw (NO) and activated (C-A) carbon.

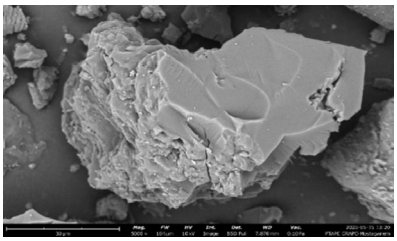


Fig. 3. The scanning electron microscopy aspect of the activated carbon.

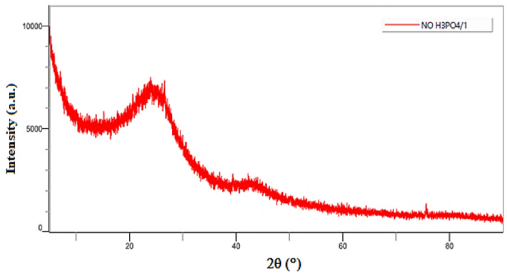


Fig. 4. XRD pattern spectrum for the Activated Carbon.

XRD analysis

The XRD pattern of the H3PO4-activated carbon is dominated by two diffuse scattering halos centered at approximately 2θ ≈ 22–25° and 2θ ≈ 42–45°, which can be assigned to the (002) and (100) reflections of turbostratic graphitic domains (Fig. 4). The breadth of these reflections is indicative of a predominantly disordered carbon structure, consistent with the disruptive effect of H3PO4 on long-range graphitic order during activation. The absence of well-defined crystalline peaks confirms that the material does not contain significant amounts of crystallized mineral phases, which is expected after effective post-activation washing. The first halo (≈ 24°) nevertheless attests to the existence of ordered but very small carbon micro-domains. Phosphoric acid activation is known to introduce oxygenated functional groups and promote the formation of micropores and mesopores, resulting in a strong structural disorder visible in the diffractogram. This amorphous microstructure, combined with an increased specific surface area, is particularly favorable for the adsorption of Tartrazine[41–43].

Quantitative XPS analysis of H_3PO_4 activated carbon reveals a surface rich in carbon (64.99%), oxygen (29.07%), and phosphorus (5.94%), confirming the effective integration and uniform incorporation of phosphorus atoms within the carbon matrix of the material. (Fig. 5). The qualitative XPS spectrum reveals the presence of characteristic peaks of C 1s, O 1s, and P 2p, reflecting a dominant aromatic carbon structure enriched in oxygenated and phosphate functional groups. The decomposition of the C 1s peak shows, in addition to the C–C and C=C bonds (~ 284.6 eV), the presence of C–O (~ 286 eV), C = O (~ 287 eV) and O–C=O (~ 288.5 eV) functional groups, associated with hydroxyls, carbonyls and carboxyls, as well as a higher energy signal (~ 290–292 eV) attributed to C–O–P bonds generated by acid activation. The O 1s spectrum confirms the coexistence of carbonyl (~ 531 eV), hydroxyls and phosphates (~ 532.5 eV), and carboxyls (~ 533.5 eV) groups, while the P 2p spectrum indicates P–O/P=O (~ 133–134 eV) and C–O–P (~ 135 eV) bonds. These results demonstrate that H_2PO_4 activation is not limited to opening the porosity, but significantly enriches the surface chemistry with polar and phosphate groups, thus improving the reactivity and adsorption capacity of Activated Carbon towards organic molecules, in particular anionic dyes such as Tartrazine[44–47]. Analysis of the graph shows that ΔpH is positive for initial pH values below 7.9 and becomes negative beyond this value (Fig. 6).

This indicates that the surface changes from a generally positive state to a negative state around pH 7.9, which corresponds to (pHpzc). This value suggests that the material has a neutral surface around pH 7.9. Thus, in an acidic environment (pH < pHpzc), the Activated Carbon surface will be positively charged, promoting the adsorption of (Tartrazine). On the other hand, at basic pH (pH > pHpzc), electrostatic repulsion can reduce the adsorption efficiency of these same anions. However, adsorption may still occur beyond the pHpzc due to alternative interaction mechanisms independent of electrostatic attraction. Even under conditions where both the adsorbent surface and the pollutant are negatively charged, non-electrostatic interactions such as π–π stacking between the aromatic rings and the graphitic structure, hydrogen bonding between surface functional groups (–OH, –COOH, $–PO_4$) and dye molecules, as well as van der Waals forces, can significantly contribute to dye uptake. In addition, the developed high specific surface area facilitates physical adsorption within micro- and mesopores, partially compensating for electrostatic repulsion. These results are consistent with the amphoteric nature of Activated Carbon surfaces and confirm the importance of pH control to optimize adsorption performance[48,49]. The significant enhancement in adsorption capacity observed in the vicinity of pH 5 can be explained by the establishment of an optimal equilibrium between the protonation state of the adsorbent surface functional groups and the degree of ionization of the dye molecules, which together favor

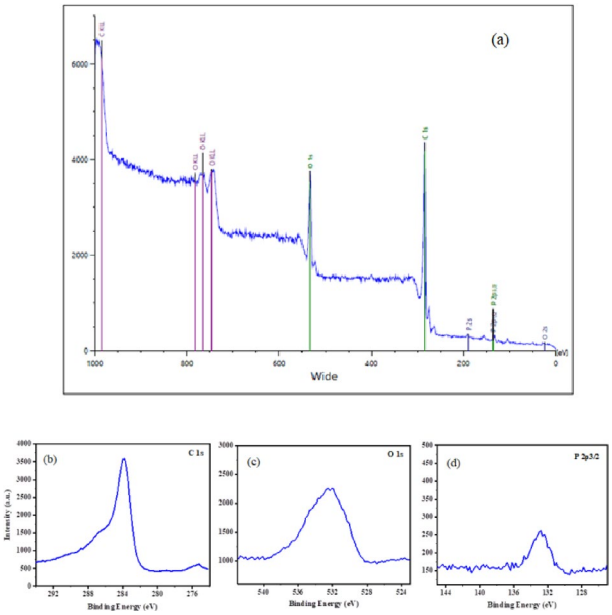


Fig. 5. The XPS spectrum of Activated Carbon. (**a**) quantitative, and qualitative of C1s (**b**), O1s (**c**) and P2p3/2 (**d**).

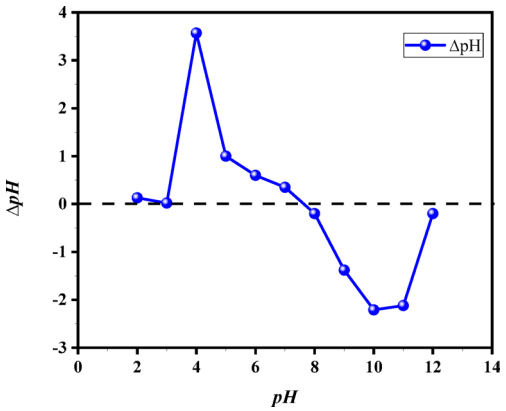


Fig. 6. The point of zero charge (pHpzc) of Activated Carbon. Experimental conditions: adsorbent dose = 0.05 g, solution volume = 50 mL, contact time = 24 h, temperature = 25 °C.

stronger electrostatic interactions and improved adsorption efficiency. At this pH, the activated carbon surface remains positively charged, enhancing electrostatic attraction, while competition from excess H^+ ions is minimized compared to strongly acidic conditions (pH ≈ 2). Furthermore, the increase observed after pH 8 may be related to the contribution of non-electrostatic interactions, such as π–π interactions between the aromatic structure and the graphitic domains, as well as possible hydrogen bonding. Even though electrostatic repulsion becomes significant above the pHpzc, these additional interaction mechanisms can partially compensate, resulting in a secondary rise in adsorption capacity. Recent studies have reported that dye adsorption on Carpobrotus edulis–based adsorbents is governed by a combination of electrostatic attraction. In particular, acid-treated *C. edulis* composites exhibited deep porous structures and active surface sites, leading to high adsorption capacities for rhodamine B and crystal violet, with equilibrium fitting the Langmuir isotherm and adsorption kinetics following the pseudo-second-order model, confirming a spontaneous adsorption process[50]. Similarly, native *C. edulis* biomass demonstrated effective crystal violet removal (Qm ≈ 86.95 mg/g), where the adsorption mechanism accompanied by exothermic and spontaneous thermodynamic behavior and reasonable regeneration stability over multiple cycles[51].

impact of various parameters on Tartrazine adsorption

The kinetic parameters obtained from the pseudo-first-order, pseudo-second-order, Elovich, and intraparticle diffusion models are presented in Table 2.

First-order			Second-order			Intraparticle			Elovich		
Qm_{cal} (mg/g)	K_1 (h^{-1})	R^2	Qm_{cal} (mg/g)	K_2(g/mg.h)	R^2	K_id (mg/g.$h^{-1/2}$)	C (J/mol)	R^2	A (mg/g.h)	B (g/mg)	R^2
4.47	0.124	0.816	31.39	0.0816	0.999	1.3076	25.34	0.815	7.49.10^6	0.59	0.889

Table 2. The kinetic parameters of the four models for Tartrazine adsorption by Activated Carbon.

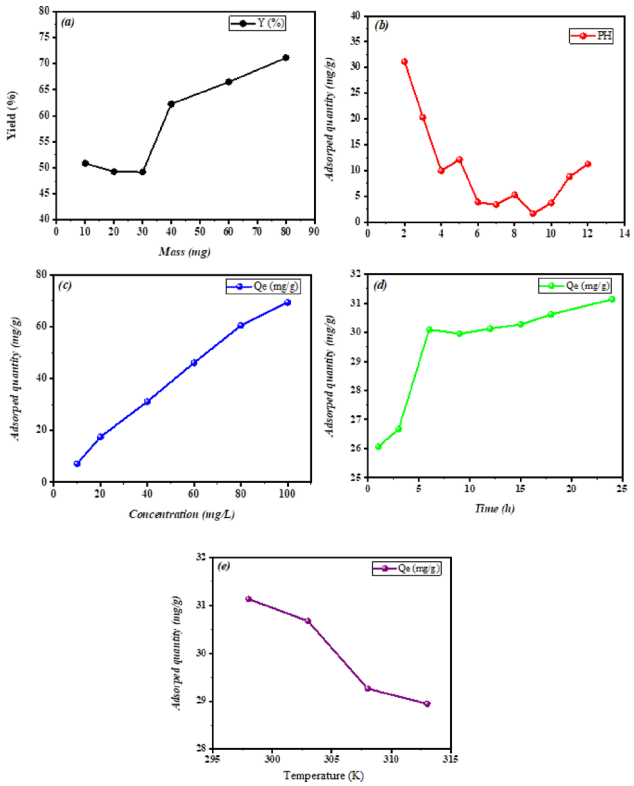


Fig. 7. Effect of some parameters on adsorption: (**a**) effect of adsorbent amount, (**b**) effect of pH, (**c**) effect of initial concentration, (**d**) effect of contact time, (**e**) effect of temperature. Experimental conditions: initial Tartrazine concentration = 40 mg/L, adsorbent dose = 40 mg, contact time = 24 h, temperature = 298 K (unless otherwise stated).

According to Table 2, the fit of pseudo-second-order model (R^2 = 0.9996), provides the best confirming that the adsorption is mainly governed by chemisorption. The investigation into the effects of operating parameters on the adsorption of Tartrazine by Activated Carbon has highlighted significant effects on the quantity adsorbed at equilibrium (Qe) (Fig. 7). Solution pH emerged as a critical determinant of adsorption efficiency: maximum uptake achieved under strongly acidic conditions (pH ≈ 2) where extensive protonation of surface sites creates a positively charged interface that favors attracts the anionic sulfonate groups of Tartrazine, whereas alkaline conditions favor OH^- competition, suppressing dye-surface interaction[52].

In addition, the adsorption behavior at intermediate pH values reflects the combined influence of electrostatic interactions and surface functional group availability. The progressive decrease in adsorption from strongly acidic to near-neutral conditions can be attributed to a reduction in surface protonation, which weakens electrostatic attraction forces. Regarding the mass of Activated Carbon, an gradual increase in the quantity of adsorbent results in a decrease in the Qe expressed in mg/g, probably due to an overabundance of unused sites and the agglomeration of particles reducing internal accessibility[53]. Increasing the initial Tartrazine concentration improves the Qe, reflecting a favorable adsorption process where the concentration gradient acts as a driver of mass transfer[54]. Although removal efficiency (%) was not plotted separately, it can be directly calculated from the adsorption capacity data. As expected, removal efficiency decreases with increasing initial dye concentration due to saturation of available active sites, while Qe increases owing to the higher driving force for mass transfer. The effect of contact time reveals a two-step kinetic process: a rapid initial adsorption phase, followed by a slowdown step beginning at 6 h, which gradually leads to a Qe plateau after 24 h[55]. Although increasing the adsorbent mass and contact time enhances dye removal, a complete saturation plateau was not strictly achieved within the investigated experimental ranges. This behavior can be attributed to gradual occupation of active sites, intraparticle diffusion resistance within the porous structure of the activated carbon, and possible particle agglomeration at higher dosages, which can significantly reduce the accessibility of the

Langmuir			Freundlich				Temkin			BET		
Qm(mg/g)	K_L(L/mg)	R^2	K_F (mg·g^{-1})(L·mg^{-1})$^{1/n}$	1/n	R^2	K_T (L/mg)	B (J/mol)	R^2	Qm(mg/g)	C	R^2
80.00	0.032	0.895	2.58	1.11	0.946	0.29	25.76	0.969	47.18	2.72	0.997

Table 3. The Modeling parameters of four isotherms models for Tartrazine adsorption by activated carbon.

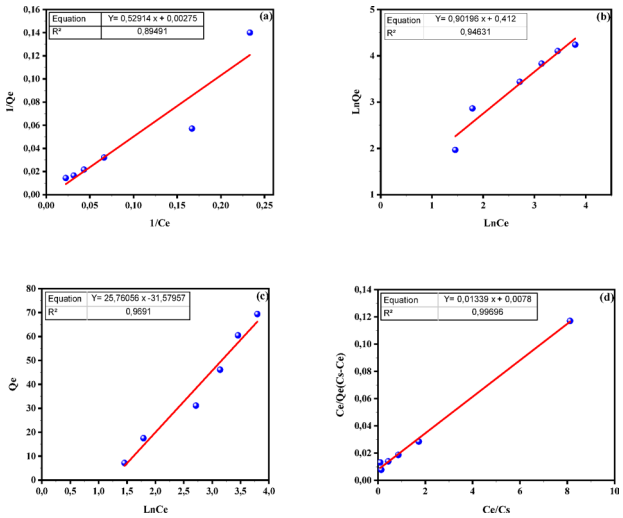


Fig. 8. Modeling of Tartrazine adsorption by Activated Carbon. (**a**) Langmuir model, (**b**) Freundlich model, (**c**) Temkin model, (**d**) BET model.

effective surface area. Moreover, longer contact times may be required to allow full diffusion of Tartrazine molecules into the internal micropores, particularly in heterogeneous multilayer adsorption systems. Finally, increasing temperature induces a decrease in Qe, indicating an exothermic process where increased thermal agitation promotes desorption, making adsorption thermodynamically less favorable at high temperatures[56]. Based on the comprehensive parametric study, the optimal operating conditions were determined as pH = 2, adsorbent dose = 40 mg, initial Tartrazine concentration = 40 mg/L, contact time = 24 h, and temperature = 298 K. These conditions were therefore selected for isotherm, kinetic, and thermodynamic investigations.

Adsorption isotherm modeling

The calculated parameters of Langmuir, Freundlich, BET, and Temkin isotherm models are summarized in Table 3. As shown in Table 2, Among the four isotherm models evaluated, the BET equation provided the most accurate description of the experimental data (R^2 = 0.997), pointing to multilayer coverage on an energetically heterogeneous surface as the prevailing adsorption mode. All adsorption isotherm parameters were recalculated and carefully verified.

According to the modeling results, the Langmuir model yielded positive constants with a maximum adsorption capacity (Qm) of 80.00 mg/g and an affinity coefficient (K_L = 0.032 L/mg), with a correlation coefficient R^2 = 0.895, indicate that monolayer adsorption may occur; however, the comparatively lower Langmuir fit quality (R^2 = 0.895) underscores the inadequacy of the monolayer homogeneous surface assumption for this system, reinforcing the heterogeneous, multilayer nature of Tartrazine adsorption. Whereas, the Freundlich model, which is empirical and adapted to heterogeneous surfaces, provided physically consistent results, with (K_F = 2.58 (mg g^{-1})(L mg^{-1})$^{1/n}$) and ($1/n$ = 1.11). The value of 1/n indicates favorable adsorption, and the high correlation coefficient (R^2 = 0.946) demonstrates a good model fit. This confirms that activated carbon exhibits a varied energy surface area and adsorption sites of varying intensities. The Temkin model, which introduces the variation of energy with surface, showed an excellent fit (R^2 = 0.969) (Fig. 8).

The constants obtained, B = 25.76 J/mol and KT = 0.29, reflect a moderate interaction, indicating the involvement of adsorbate–adsorbent interactions. Finally, the BET model, adapted to multilayer adsorption, provided the best fit with an exceptional correlation coefficient (R^2 = 0.997). The calculated maximum capacity (Qm = 47.18 mg g^{-1}) and the energy constant C = 2.72 are consistent with progressive adsorption over multiple layers, which is typical of microporous or mesoporous surfaces such as that of the prepared Activated Carbon. These results confirm that multilayer adsorption on a heterogeneous surface is the dominant mechanism, governed mainly by successive Van der Waals interactions[57–60]. The BET-derived maximum capacity (47.18 mg g^{-1}) falls within the performance range documented for analogous agricultural waste-based carbons used in dye removal applications (35–55 mg g^{-1}), confirming the competitive adsorptive potential of the prepared material[61]. The Qm obtained from the Langmuir model (Qm = 80.00 mg g^{-1}) is higher than that calculated from the BET model (Qm = 47.18 mg g^{-1}). This difference arises from the Langmuir assumption of monolayer adsorption

Adsorbent	Pollutant	Qm (mg g^{-1})	Dominant Isotherm	pH	References
Activated carbon (olive pits) (this work)	Tartrazine	47.18	BET / Freundlich	2	This work
Sawdust (agricultural waste)	Tartrazine	4.71	Langmuir	3	[62]
Activated carbon from cassava sievate	Tartrazine	20.83	Langmuir / Freundlich	1–2	[63]
Commercial biochar	Tartrazine	3.28	Langmuir	-	[64]

Table 4. Comparison of Tartrazine adsorption performance with open-access literature.

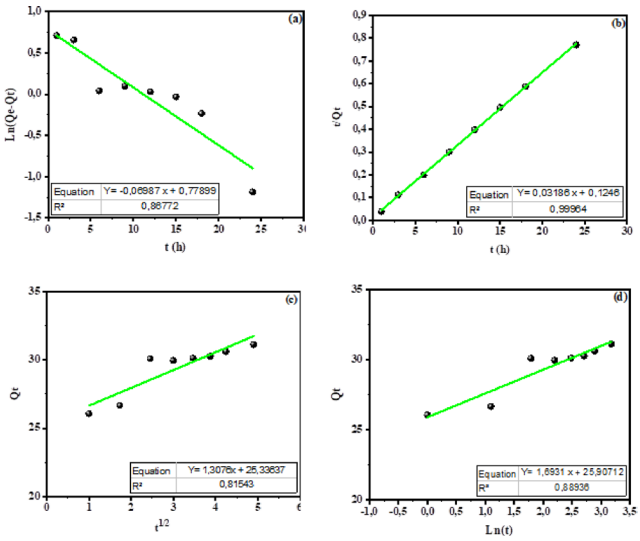


Fig. 9. Kinetic models of Tartrazine adsorption onto Activated Carbon: (**a**) pseudo-first-order, (**b**) pseudo-second-order, (**c**) intraparticle diffusion, and (**d**) Elovich models.

on homogeneous sites, which tends to overestimate capacity in heterogeneous systems. In contrast, the BET model considers the possibility for multilayer adsorption and therefore provides a more realistic representation description of the adsorption behavior exhibited of activated carbon material. A comparison of the adsorption performance of the prepared activated carbon with selected open-access reports on Tartrazine removal is presented in Table 4.

As shown in Table 4, the Qm of this adsorbent is significantly higher than adsorbents such as sawdust and commercial biochar. The activated carbon derived from cassava sievate also shows an appreciable Qm. however, it is lower than the value of activated carbon derived from pits olive. Variations in Qm and dominant isotherm models are attributed to differences in precursor material, activation method, surface chemistry, and experimental conditions including pH and initial concentration. Beyond dye adsorption studies, recent research has explored a coconut shell-derived nanomagnetic biocarbon composite was recently developed for turbidity removal in drinking water[62–65]. The study demonstrated enhanced adsorption efficiency and improved surface functionality through nanoparticle impregnation. Although the target pollutant differs from Tartrazine, both studies highlight the effectiveness of biomass-derived carbon materials with developed porosity and heterogeneous surface characteristics. The differences in adsorption capacity are attributed to pollutant nature, measurement units, and surface modification strategies.

Adsorption kinetics and thermodynamic studies

the kinetic models tested, the ($R^2 = 0.9996$) of pseudo-second-order model is the best compared to $R^2 = 0.818$, $R^2 = 0.818$, and $R^2 = 0.813$ for the first-order, Elovich, and intraparticle models, respectively (Fig. 9).

The results of kinetic implies that surface-chemical interactions-likely involving coordination between Tartrazine and specific functional groups constitute the rate-governing step, consistent with a chemisorption mechanism. The Qm obtained from this model nearly identical to the experimental value, which reinforces the validity of the model. The rate constant $K_2 = 0.0816$ g mg^{-1} h^{-1} reflects relatively fast adsorption kinetics. In contrast, the first-order model, the intraparticle diffusion model, and the Elovich model showed less satisfactory fit, suggesting that these models do not adequately describe the adsorption rate in this system[66–70]. Based on kinetic, isotherm, thermodynamic, and surface characterization results, the adsorption mechanism of Tartrazine onto H_2PO_4-activated carbon can be described as a mixed process where physisorption predominates. Although the pseudo-second-order kinetic model achieved the best correlation, the relatively low enthalpy value ($\Delta H° \approx -10.3$ kJ/mol) and BET multilayer adsorption behavior indicate that physical interactions are predominant. Electrostatic attraction under acidic conditions, π–π interactions between aromatic structures, hydrogen bonding with surface functional groups (–OH, –COOH, $–PO_4$), and van der Waals forces mainly govern the

ΔH° (J/mol)	ΔS° (J/mol.K)	ΔG° (J/mol)				R^2
		298 K	303 K	308 K	313 K	
−10,328	−28.58	−1809.76	−1666.84	−1523.92	−1381.01	0.938

Table 5. The thermodynamic parameters of Tartrazine adsorption by activated carbon.

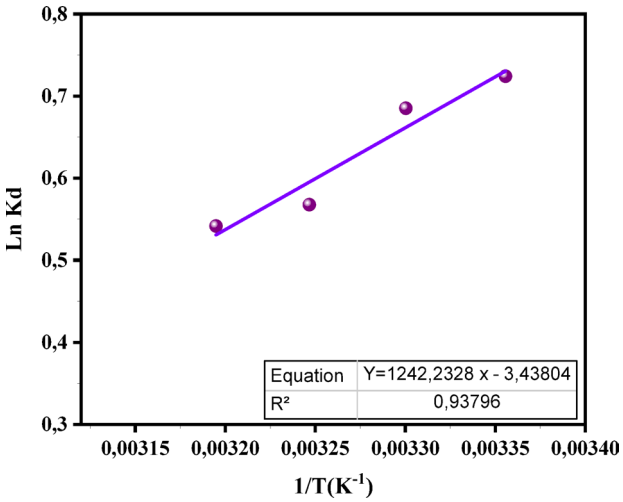


Fig. 10. Thermodynamic analysis of Tartrazine adsorption onto Activated Carbon.

adsorption process, while weak chemisorption through surface functional groups may also contribute. The thermodynamic parameters are listed in Table 5.

Negative Gibbs free energy values across the studied temperature range (298–313 K) confirm the thermodynamically spontaneous character of Tartrazine adsorption under the investigated conditions. (Fig. 10). The sign negative of enthalpy (ΔH° = -10328 J mol^{-1}) establishes the exothermic interaction and accounts for the observed inverse relationship between temperature and adsorption capacity a hallmark of physisorption interactions, where interaction forces are generally weak (Van der Waals interactions or hydrogen bonds). The sign negative of entropy term (ΔS° = – 28.58 J/mol K) reflects a diminution in system disorder upon adsorption, attributable to the ordered arrangement adopted by Tartrazine molecules at the solid-liquid interface. Overall, these results confirm that the adsorption mechanism is mainly physical and favorable at room temperature[71–74]. Although the results of the kinetic study suggest that the adsorption process follows a mechanism commonly associated with chemisorption, this does not necessarily imply pure chemisorption. but rather suggests the coexistence of both chemical and physical interactions. While surface functional groups may contribute to specific interactions with Tartrazine molecules, the relatively low negative ΔH° value indicates that physisorption plays a dominant role. Therefore, the adsorption phenomenon can be described as a mixed mechanism involving both physisorption and weak chemisorptions. The sign negative of ΔG° at all investigated temperatures demonstrated the spontaneous of Tartrazine adsorption onto activated carbon. These thermodynamic findings are consistent with the kinetic results and support the proposed mixed adsorption mechanism.

The adsorption mechanism of Tartrazine onto H_2PO_4-activated carbon is governed by multiple interactions. At acidic pH (pH < pHpzc), the surface of carbon becomes positively charged, thereby enhancing strong electrostatic attraction and π–π interactions. Hydrogen bonding between surface oxygen-containing functional groups (–OH, –COOH, $–PO_4$) and dye molecules also contributes to adsorption. Furthermore, van der Waals forces facilitate multilayer adsorption, as confirmed by the BET isotherm model. Therefore, the overall adsorption process follows a mixed mechanism dominated by physisorption with a minor contribution of chemisorption.

Conclusion

The present work establishes olive pits a abundantly available agro-industrial residue as an effective and sustainable precursor for producing activated carbon with high Tartrazine removal efficiency from water. H3PO4 mediated activation yielded a microporous amorphous carbon material with an enriched surface chemistry featuring oxygenated and phosphate groups that markedly amplified the adsorbent-dye interaction strength. Characterization by FTIR, SEM, XRD, and XPS confirmed successful carbonization and activation, revealing a heterogeneous morphology and a chemically reactive surface. Batch adsorption experiments highlighted that the process strongly depends on pH, contact time, initial dye concentration, adsorbent dose, and temperature. Maximum adsorption occurred in acidic conditions and decreased with temperature, confirming the exothermic process. Kinetic modeling indicated that the pseudo-second-order model describes the prosses with a best fits the data (R^2 = 0.999), indicating a mixed mechanism dominated by physisorption with a minor contribution of chemisorption. The Freundlich, Temkin, and especially BET isotherms provided the best fits (R^2 = 0.946, 0.969,

and 0.997, respectively), demonstrating multilayer adsorption on a heterogeneous surface, with a BET maximum adsorption capacity of 47.18 mg g^{-1}, while the Langmuir model yielded a higher theoretical Qm of 80.00 mg g^{-1}. Thermodynamic analysis revealed negative ΔG° values, confirming the spontaneous process, while the negative ΔH° value indicated an exothermic interaction. These findings validate that the H_2PO_4- Activated Carbon derived from olive pits is an efficient, and a low-cost, and sustainable adsorbent for dye removal. In conclusion, olive pit–based Activated Carbon represents a economical, and high-performance adsorbent for the efficient removal of Tartrazine. Its use promotes agricultural waste valorization and environmental protection. After adsorption, the spent activated carbon can be regenerated by thermal treatment or solvent washing for potential reuse. If regeneration is not feasible, the exhausted adsorbent may be safely disposed of through controlled incineration or stabilization followed by landfilling in accordance with environmental regulations, thereby minimizing secondary pollution risks. Despite the promising results obtained in this study, some limitations should be acknowledged. The adsorption experiments were conducted using synthetic dye solutions under batch conditions, and real industrial wastewater was not investigated. In addition, regeneration and reuse were discussed but not experimentally evaluated. Future work should therefore focus on column studies, regeneration cycles, economic assessment, and application to real effluents to further validate the practical feasibility of the developed adsorbent.

Data availability

Data underlying the results presented in this paper are not publicly available at this time but may be obtained from the corresponding author (fatmimessaud@yahoo.fr) upon reasonable request.

Received: 29 October 2025; Accepted: 31 May 2026
Published online: 05 June 2026

References

1. Chen, X. et al. Elevated efficiency in tartrazine removal from wastewater through boron-doped biochar: Enhanced adsorption and persulfate activation. *Biochar* **6**, 79. https://doi.org/10.1007/s42773-024-00377-4 (2024).
2. Boyer, E. et al. Prenatal exposure to persistent organic pollutants and molar-incisor hypomineralization among 12-year-old children in the French mother-child cohort PELAGIE. *Environ. Res.* **231** (Pt 3), 116230. https://doi.org/10.1016/j.envres.2023.116230 (2023).
3. Ozcan, D. O., Hendekci, M. C. & Ovez, B. Enhancing the adsorption capacity of organic and inorganic pollutants onto impregnated olive stone derived activated carbon. *Heliyon* **10** (12), e32792. https://doi.org/10.1016/j.heliyon.2024.e32792 (2024).
4. Khatoon, A., Siddiqui, S., Khan, S. H., Alfaiz, F. A. & Uddin, M. K. Removal of methylene blue, crystal violet, and diclofenac sodium using cellulose derived from *Luffa acutangula* peels: Adsorption, reusability, and cost evaluation. *Biomass Convers. Biorefin.* **15**, 30995–31008. https://doi.org/10.1007/s13399-025-06883-0 (2025).
5. Uddin, M. K. & Nasar, A. Decolorization of basic dyes solution by utilizing fruit seed powder. *KSCE J. Civ. Eng.* **24**, 345–355. https://doi.org/10.1007/s12205-020-0523-2 (2020).
6. Siddiqui, S. H., Uddin, M. K., Isaac, R., Aldosari, O. F. & Chen, Q. An effective biomass for the adsorption of methylene blue dye and treatment of river water. *Adsorpt. Sci. Technol.* 4143138. https://doi.org/10.1155/2022/4143138 (2022).
7. Uddin, M. K., Abd Malek, N. N., Jawad, A. H. & Sabar, S. Pyrolysis of rubber seed pericarp biomass treated with sulfuric acid for adsorption of crystal violet and methylene green dyes. *Int. J. Phytoremediat.* **25**, 393–402. https://doi.org/10.1080/15226514.2022.2086214 (2023).
8. Afshin, S. et al. Eco-friendly synthesis of ZnO nanoparticles loaded on tire-derived activated carbon for dye removal. *Desalin. Water Treat.* **227**, 391–403. https://doi.org/10.5004/dwt.2021.27283 (2021).
9. Pourali, P. et al. Dissociation of acid blue 113 dye from aqueous solutions using activated persulfate by zero iron nanoparticle from green synthesis: The optimization process with RSM-BBD model: Mineralization and reaction kinetic study. *Biomass Convers. Biorefin.* **14**, 6333–6345. https://doi.org/10.1007/s13399-022-02942-y (2024).
10. Mahdavian, F., Rahmani, A. R., Rahmani, H., Nouri, J. & Khataee, Enhanced removal of cefixime using Fe_3O_4@GO nanocomposite with ultrasonic assistance. *Desalin. Water Treat.* **280**, 224–239. https://doi.org/10.5004/dwt.2022.29111 (2022).
11. Rashtbari, Y., Hazrati, S., Vosoughi, M., Ghasemi, S. M. & Fazlzadeh, M. Potential of green adsorbent for humic acid removal. *Int. J. Environ. Anal. Chem.* **102**, 5373–5390. https://doi.org/10.1080/03067319.2020.1796993 (2022).
12. Parastar, S., Rashtbari, Y., Hazrati, S., Vosoughi, M. & Fazlzadeh, M. Efficiency of methylene blue removal using iron magnetic nanoparticles on clinoptilolite. *Int. J. Environ. Res.* **19**, 35. https://doi.org/10.1007/s41742-024-00702-6 (2025).
13. Salimifard, A., Rashtbari, Y., Hazrati, S., Vosoughi, M. & Fazlzadeh, M. Furfural removal using modified nanoclay with nZVI. *Int. J. Environ. Res.* **19**, 232. https://doi.org/10.1007/s41742-025-00878-5 (2025).
14. Ahmadfazeli, A., Rashtbari, Y., Hazrati, S., Vosoughi, M. & Fazlzadeh, M. Removal of metronidazole by ammonia-modified activated carbon. *J. Water Sanit. Hyg. Dev.* **11**, 1083–1096. https://doi.org/10.2166/washdev.2021.117 (2021).
15. Kali, A., Rashidi Nodeh, H., Sereshti, H. & Rashidi, A. M. Low-cost shell adsorbents for copper removal. *Biomass Convers. Biorefin.* **14**, 3655–3666. https://doi.org/10.1007/s13399-022-02564-4 (2024).
16. Loulidi, I. et al. Role of electrostatic and π–π interactions in the removal of crystal violet and reduction of Cr(VI) ions from aqueous solutions using spent coffee grounds. *J. Water Process. Eng.* **77**, 108578. https://doi.org/10.1016/j.jwpe.2025.108578 (2025).
17. Imame, S. et al. Efficient adsorption of malachite green from wastewater using agricultural biosource waste: Kinetic, isothermal, thermodynamic studies and mechanisms analysis. *Methods Environ. Chem. J.* **8** (1), 5–25. https://doi.org/10.24200/amecj.v8.i01.359 (2025).
18. Sadoq, M. et al. Utilization of argan nut shells as a bioresource for efficient malachite green oxalate adsorption. *Chem. Pap.* **78**, 7525–7540. https://doi.org/10.1007/s11696-024-03611-2 (2024).
19. Mahmoudy, G. et al. Preparation and characterization of biomaterial for phosphate ion removal: Kinetics, isotherms and thermodynamics studies. *Desalin. Water Treat.* **317**, 100062. https://doi.org/10.1016/j.dwt.2024.100062 (2024).
20. Alshahrani, H., Abdulhameed, A. S., Khan, M. K. A., Al Omari, R. H. & Algburi, S. Functionalization of chitosan/alumina nanoparticles with carboxylic groups using phthalic anhydride for adsorption of methylene blue dye via response surface methodology. *Polym Bull.* ;82:87–109. (2025). Available from: https://doi.org/10.1007/s00289-024-05522-4
21. Dabagh, A. et al. Remediation of hazardous dyes on low-cost biosorbent: Batch and dynamic adsorption, phytotoxicity assessment, and application of industrial wastewater. *Biomass Convers. Biorefin.* **15**, 19751–19769. https://doi.org/10.1007/s13399-025-06531-7 (2025).

22. Jamrah, A., AlJawaldeh, H., AlZghoul, T. M., AlShannag, M. & Al-Salaymeh, A. Olive pits activated carbon as an effective adsorbent for water treatment using H_3PO_4 and H_2SO_4 activating agents. *Water Conserv. Manage.* **4**, 415–419. https://doi.org/10.26480/wcm.04.2024.415.419 (2024).
23. Mbarek, M., Jedli, H., Rabhi, R. & Slimi, K. Activated carbon derived from olive waste for the adsorption of methylene blue and methyl orange dyes. *ChemistrySelect.* ;9:e202404066. (2024). Available from: https://doi.org/10.1002/slct.202404066
24. Iles, A., Zaoui, F., Elhadj Daouadji, B., Bensalah, N. & Belkacemi, K. Removal of pollutants by olive stones derived activated carbon@Fe_3O_4 nanocomposites: Effect of calcination temperature on adsorption properties. *J. Water Process. Eng.* **58**, 105960. https://doi.org/10.1016/j.jwpe.2024.105960 (2024).
25. Ma, X., Hou, Y., Yang, L. & Lv, H. Adsorption behaviors of VOCs under coal-combustion flue gas environment using activated carbon injection coupled with bag filtering system. *Colloids Surf. Physicochem Eng. Asp.* **627**, 127158. https://doi.org/10.1016/j.colsurfa.2021.127158 (2021).
26. Goldstein, J. et al. *Scanning Electron Microscopy and X-ray Microanalysis* 4th edn (Springer, 2018). https://doi.org/10.1007/978-1-4939-6676-9
27. Li, Y., Zhang, T. & Wang, H. Structural characterization of activated carbons by XRD and its relationship with adsorption performance. *J. Mater. Res. Technol.* **18**, 1452–1461. https://doi.org/10.1016/j.jmrt.2022.04.059 (2022).
28. Li, Y., Li, X. & Liu, H. Surface chemistry of activated carbons characterized by XPS and its correlation with adsorption properties. *J. Environ. Chem. Eng.* **11**, 109876. https://doi.org/10.1016/j.jece.2023.109876 (2023).
29. Liu, Y., Liu, G., Wang, X. & Wang, S. Determination of point of zero charge (pHpzc) of biochars and its influence on adsorption performance: A critical review. *J. Environ. Chem. Eng.* **10**, 107084. https://doi.org/10.1016/j.jece.2021.107084 (2022).
30. Lee, G., Ahmed, I., Lee, H. J. & Jhung, S. H. Adsorptive removal of organic pollutants with a specific functional group from water by using metal–organic frameworks (MOFs) or MOF-derived carbons: A review. *Sep. Purif. Technol.* **347**, 127602. https://doi.org/10.1016/j.seppur.2024.127602 (2024).
31. Ozcelik, T. O. et al. Methylene blue removal using activated carbon from olive pits: Response surface approach and artificial neural network. *Processes* **13**, 347. https://doi.org/10.3390/pr13020347 (2025).
32. Honorine, A. T., Daouda, A., Domga, T., Domga, R. & Noumi, G. B. Efficient adsorption of tartrazine from an aqueous solution using a low-cost orange peel powder. *J. Water Health.* **21**, 1017–1031. https://doi.org/10.2166/wh.2023.033 (2023).
33. Dessie, W., Luo, X., Duns, G. J., Wang, M. & Qin, Z. Towards the development of efficient, economic and environmentally friendly downstream processing for bio-based succinic acid. *Sep. Purif. Technol.* **347**, 127602. https://doi.org/10.1016/j.seppur.2024.127602 (2024).
34. Amaku, J. F. et al. Aqueous phase removal of tartrazine: Review of kinetics, isotherms, and thermodynamics. *Chem. Afr.* **7**, 1685–1705. https://doi.org/10.1007/s42250-023-00832-y (2024).
35. Tejada-Tovar, C., Villabona Ortiz, Á., Aguilar Bermúdez, F., Pájaro Moreno, Y. & González Delgado, Á. D. Evaluation of adsorbent biomaterials based on coconut mesocarp for treatment of wastewater contaminated with tartrazine dye. *Processes* **11**, 3115. https://doi.org/10.3390/pr11113115 (2023).
36. Ioannidou, O. & Zabaniotou, A. Agricultural residues as precursors for activated carbon production. *Renew. Sustain. Energy Rev.* **11**, 1966–2005. https://doi.org/10.1016/j.rser.2006.03.013 (2007).
37. Yakout, S. M. Removal of benzene from aqueous solution using phosphoric acid activated carbon from rice husk. *Chem. Cent. J.* **8**, 52. https://doi.org/10.1186/s13065-014-0052-5 (2014).
38. Al-Ghouti, M. A. & Da'ana, D. A. Guidelines for the use and interpretation of adsorption isotherm models: A review. *J. Hazard. Mater.* **393**, 122383. https://doi.org/10.1016/j.jhazmat.2020.122383 (2020).
39. Foo, K. Y. & Hameed, B. H. Insights into the modeling of adsorption isotherm systems. *Chem. Eng. J.* **431**, 134322. https://doi.org/10.1016/j.cej.2021.134322 (2022).
40. Mohseninia, N., Memarian, N. & Rezagholipour Dizaji, H. Theoretical investigation of adsorptive nitrate ion removal by pure graphene, Mo-decorated graphene and reduced graphene oxide based adsorbents: a DFT study. *J Appl Crystallogr.* ;58:194–206. (2025). Available from: https://doi.org/10.1107/S1600576725000032
41. Ji, K., Sheng, F., Liu, T., Das, B. & Buonassisi, T. Multimodal transformers with elemental priors for phase classification of X-ray diffraction spectra. *arXiv* https://doi.org/10.48550/arXiv.2505.09536 (2025).
42. Pal, D., Wang, Y., Gurunathan, R. & Dresselhaus Marais, L. Measuring the Burgers vector of dislocations with dark field X-ray microscopy. *J. Appl. Crystallogr.* **58**, 221–226. https://doi.org/10.1107/S1600576725000342 (2025).
43. Wang, X. & Spratt, H. Incorporating the direct derivation method and molecular scattering power method into the Rietveld quantitative phase analysis routine in TOPAS. *J. Appl. Crystallogr.* **58**, 1174–1184. https://doi.org/10.1107/S1600576725004376 (2025).
44. Baer, D. R. et al. What more can be done with XPS? Highly informative, but underused approaches to XPS data collection and analysis. *J. Vac Sci. Technol. A.* **43**, 060045. https://doi.org/10.1116/6.0004543 (2025).
45. Jiménez Arévalo, N. et al. X-ray photoelectron spectroscopy of high-throughput mechanically exfoliated van der Waals materials. *Nanoscale* **16**, 17559–17566. https://doi.org/10.1039/D4NR02882A (2024).
46. Gu, Y. et al. Extending ambient pressure X-ray photoelectron spectroscopy to plasma studies: A novel and flexible plasma gun approach. *arXiv* https://doi.org/10.48550/arXiv.2503.11446 (2025).
47. Diulus, J.T., Head, A.R., Boscoboinik, J.A. & Kolmakov, A. Operando XPS in reactive plasmas: The importance of the wall reactions. *arXiv* https://doi.org/10.48550/arXiv.2502.19303 (2025).
48. Gutierrez-Martinez, J. et al. Point of zero charge, isoelectric point, and potential of zero charge on activated carbons: A comprehensive interpretation about their interrelation. *Curr. Opin. Solid State Mater. Sci.* **40**, 101247. https://doi.org/10.1016/j.cossms.2025.101247 (2026).
49. Neupane, S. et al. An alternative pH sensor: Graphene oxide-based electrochemical sensor. *Emergent Mater.* **5**, 509–517. https://doi.org/10.1007/s42247-021-00238-x (2022).
50. Dabagh, A. et al. Enhanced cationic/anionic dyes removal in wastewater by green nanocomposites synthesized from acid-modified biomass and $CuFe_2O_4$ nanoparticles. *Environ. Nanotechnol Monit. Manag.* **22**, 101019. https://doi.org/10.1016/j.enmm.2024.101019 (2024).
51. Belkassa, K., Khelifa, M., Batonneau-Gener, I., Marouf-Khelifa, K. & Khelifa, A. Understanding of the mechanism of crystal violet adsorption on modified halloysite: Hydrophobicity, performance, and interaction. *J. Hazard. Mater.* **415**, 125656. https://doi.org/10.1016/j.jhazmat.2021.125656 (2021).
52. Yirdaw, G. Efficient removal of lead (II) from paint factory wastewater using Noug stalk activated carbon: A sustainable adsorption approach. *Heliyon* **11**, e42281. https://doi.org/10.1016/j.heliyon.2025.e42281 (2025).
53. Tahir, S. S. & Rauf, N. Removal of a cationic dye from aqueous solutions by adsorption onto bentonite clay. *Chemosphere* **63** (11), 1842–1848. https://doi.org/10.1016/j.chemosphere.2005.10.033 (2006).
54. Wiśniewska, M. The temperature effect on the adsorption mechanism of polyacrylamide on the silica surface and its stability. *Appl. Surf. Sci.* https://doi.org/10.1016/j.apsusc.2011.11.044 (2011). 11.044.
55. Jung, K. W. et al. Adsorptive removal of anionic azo dye from aqueous solution using activated carbon derived from extracted coffee residues. *J Clean Prod.* ;166:360–368. (2017). Available from: https://doi.org/10.1016/j.jclepro.2017.08.045
56. Alkan, M., Demirbaş, Ö. & Doğan, M. Adsorption kinetics and thermodynamics of an anionic dye onto sepiolite. *Microporous Mesoporous Mater.* ;101(3):388–396. (2007). Available from: https://doi.org/10.1016/j.micromeso.2006.12.007

57. Aita, S. A. et al. Investigating adsorption of aqueous heavy metals through isotherms and kinetics with Zn–Co–Fe/LDH for remarkable removal efficiency. *Appl Water Sci.* ;15(4):75. (2025). Available from: https://doi.org/10.1007/s13201-025-02390-9
58. Huang, Y. T. & Shih, M. C. Kinetic, isotherm, and thermodynamic modeling of methylene blue adsorption using natural rice husk: A sustainable approach. *Separations* **12**, 189. https://doi.org/10.3390/separations12080189 (2025).
59. Najm, K. & Naser, O. A. Adsorption efficiency investigation of polyacrylonitrile for methyl green dye from aqueous solution. *Ibn Al Haitham J. Pure Appl. Sci.* **38**, 251–262. https://doi.org/10.30526/38.1.3520 (2025).
60. Calvete, T. et al. Application of carbon adsorbents prepared from Brazilian-pine fruit shell for the removal of reactive orange 16 from aqueous solution: Kinetic, equilibrium, and thermodynamic studies. *J Environ Manage.* ;91(8):1695–1706. (2010). Available from: https://doi.org/10.1016/j.jenvman.2010.03.013
61. Demiral, H. & Güngör, H. Adsorption of copper(II) ions on activated carbon prepared from grape bagasse. *J. Clean. Prod.* **124**, 103–113. https://doi.org/10.1016/j.jclepro.2016.02.084 (2016).
62. Banerjee, S. & Chattopadhyaya, M. C. Adsorption of tartrazine from aqueous solutions by a low cost agricultural by-product. *Arab. J. Chem.* **10** (Suppl 2), S1629–S1638. https://doi.org/10.1016/j.arabjc.2013.06.005 (2017).
63. Chukwuemeka-Okorie, H. O. et al. Adsorption of tartrazine and sunset yellow onto activated carbon derived from cassava sievate biomass. *Appl Water Sci.* ;11:27. (2021). Available from: https://doi.org/10.1007/s13201-021-01357-w
64. Soran, M. L. et al. Commercially biochar applied for tartrazine removal from aqueous solutions. *Appl Sci.* ;14:53. (2024). Available from: https://doi.org/10.3390/app14010053
65. Awang, H. et al. Coconut shell-derived biocarbon composite for adsorptive field-water purification. *Mater Chem Phys.* ;333:130359. (2025). Available from: https://doi.org/10.1016/j.matchemphys.2025.130359
66. Aboussabek, A. et al. Experimental investigation, kinetics and statistical modeling of methylene blue removal onto Clay@Fe_3O_4: Batch, fixed bed column adsorption and photo-Fenton degradation studies. *Case Stud Chem Environ Eng.* ;9:100580. (2024). Available from: https://doi.org/10.1016/j.cscee.2023.100580
67. Boudinar, M. et al. Adsorption isotherm and kinetic modeling of malachite green dye on cost-effective mesoporous material Al MCM-41 synthesized from local clay. *React Kinet Mech Catal.* ;137:2331–2348. (2024). Available from: https://doi.org/10.1007/s11144-024-02636-8
68. Demehin, A. I., Awotunde, J. O. & Oke, I. I. Properties of surface water: Adsorption kinetics and mechanism of arsenic and lead ions removal using a matrix technique. *FUDMA J Sci.* ;9:74–86. (2025). Available from: https://doi.org/10.33003/fjs-2025-0901-2852
69. Magdy, A., Mostafa, M. R., Moustafa, S. A., Mohamed, G. G. & Fouad, O. A. Kinetics and adsorption isotherms studies for the effective removal of Evans blue dye from an aqueous solution utilizing forsterite nanoparticles. *Sci Rep.* ;14:24392. (2024). Available from: https://doi.org/10.1038/s41598-024-73697-x
70. Onursal, N. et al. Application of a new adsorption kinetic model for the removal of Zn(II) ions present in aqueous solutions with Malatya clay. *J King Saud Univ Sci.* ;37:102888. (2025). Available from: https://doi.org/10.25259/JKSUS_423_2024
71. Yang, X. & Zhao, F. Adsorption thermodynamics and kinetics of hydrochloric-acid-modified bentonite for Zn(II) in wastewater. *Desalin Water Treat.* ;317:100279. (2024). Available from: https://doi.org/10.1016/j.dwt.2024.100279
72. Duan, S., Xie, Y., Shen, S. & Li, G. D. Comparative analysis of CO_2 and N_2 adsorption on zeolite 4A: Thermodynamics parameters and site energy distribution investigations. *J Environ Chem Eng.* ;12:112870. (2024). Available from: https://doi.org/10.1016/j.jece.2024.112870
73. Iqajtaoune, A., Taibi, M., Saufi, H., Aouan, B. & Boudad, L. Enhanced removal of methylene blue and procion deep red H-EXL dyes from aqueous environments by modified-bentonite: Isotherm, kinetic, and thermodynamic studies. *Desalin Water Treat.* ;320:100607. (2024). Available from: https://doi.org/10.1016/j.dwt.2024.100607
74. Fang, N. et al. Insight into adsorption kinetics, equilibrium, thermodynamics, and modeling of ciprofloxacin onto iron ore tailings. *Water.* ;17:760. (2025). Available from: https://doi.org/10.3390/w17050760

Acknowledgements

The authors would like to acknowledge the Deanship of Graduate Studies and Scientific Research, Taif University for funding this work.

Author contributions

Conceptualization: Abderrahmane Remil, Abdelkrim Bendoukha Reguig, Mokhtar Saidi, Formal analysis: Abdelghani Bouchama, Mohammed El Amine Monir, S. Alomairy, Talal M Algathfi, Aseel Smerat, Mustafa Jaipallah Abdelmageed Abualreishh, Murat Yaylacı, Validation: M. Fatmi.

Funding

The authors would like to acknowledge the Deanship of Graduate Studies and Scientific Research, Taif University for funding this work.

Declarations

Competing interest

The authors declare no competing interest.

Additional information

Correspondence and requests for materials should be addressed to M.F.

Reprints and permissions information is available at www.nature.com/reprints.

Publisher's note Springer Nature remains neutral with regard to jurisdictional claims in published maps and institutional affiliations.

Open Access This article is licensed under a Creative Commons Attribution-NonCommercial-NoDerivatives 4.0 International License, which permits any non-commercial use, sharing, distribution and reproduction in any medium or format, as long as you give appropriate credit to the original author(s) and the source, provide a link to the Creative Commons licence, and indicate if you modified the licensed material. You do not have permission under this licence to share adapted material derived from this article or parts of it. The images or other third party material in this article are included in the article's Creative Commons licence, unless indicated otherwise in a credit line to the material. If material is not included in the article's Creative Commons licence and your intended use is not permitted by statutory regulation or exceeds the permitted use, you will need to obtain permission directly from the copyright holder. To view a copy of this licence, visit http://creativecommons.org/licenses/by-nc-nd/4.0/.

© The Author(s) 2026, modified publication 2026